



# NAD(H)-mediated tetramerization controls the activity of *Legionella pneumophila* phospholipase PlaB

Maurice Diwo<sup>a,1</sup>, Wiebke Michel<sup>b,1</sup>, Philipp Aurass<sup>b</sup>, Katja Kuhle-Keindorf<sup>b</sup>, Jan Pippel<sup>a</sup>, Joern Krausze<sup>a</sup>, Sabrina Wamp<sup>b</sup>, Christina Lang<sup>b</sup>, Wulf Blankenfeldt<sup>a,c,2,3</sup>, and Antje Flieger<sup>b,2,3</sup>

<sup>a</sup>Structure and Function of Proteins, Helmholtz Centre for Infection Research, 38124 Braunschweig, Germany; <sup>b</sup>Division of Enteropathogenic Bacteria and Legionella, Robert Koch Institute, 38855 Wernigerode, Germany; and <sup>c</sup>Institute for Biochemistry, Biotechnology and Bioinformatics, Technische Universität Braunschweig, 38106 Braunschweig, Germany

Edited by Kim Orth, The University of Texas Southwestern Medical Center, Dallas, TX, and approved April 22, 2021 (received for review August 11, 2020)

The virulence factor PlaB promotes lung colonization, tissue destruction, and intracellular replication of *Legionella pneumophila*, the causative agent of Legionnaires' disease. It is a highly active phospholipase exposed at the bacterial surface and shows an extraordinary activation mechanism by tetramer deoligomerization. To unravel the molecular basis for enzyme activation and localization, we determined the crystal structure of PlaB in its tetrameric form. We found that the tetramer is a dimer of identical dimers, and a monomer consists of an N-terminal  $\alpha/\beta$ -hydrolase domain expanded by two noncanonical two-stranded  $\beta$ -sheets,  $\beta$ -6/ $\beta$ -7 and  $\beta$ -9/ $\beta$ -10. The C-terminal domain reveals a fold displaying a bilobed  $\beta$ -sandwich with a hook structure required for dimer formation and structural complementation of the enzymatic domain in the neighboring monomer. This highlights the dimer as the active form.  $\Delta\beta$ -9/ $\beta$ -10 mutants showed a decrease in the tetrameric fraction and altered activity profiles. The variant also revealed restricted binding to membranes resulting in mislocalization and bacterial lysis. Unexpectedly, we observed eight NAD(H) molecules at the dimer/dimer interface, suggesting that these molecules stabilize the tetramer and hence lead to enzyme inactivation. Indeed, addition of NAD(H) increased the fraction of the tetramer and concomitantly reduced activity. Together, these data reveal structural elements and an unprecedented NAD(H)-mediated tetramerization mechanism required for spatial and enzymatic control of a phospholipase virulence factor. The allosteric regulatory process identified here is suited to fine tune PlaB in a way that protects *Legionella pneumophila* from self-inflicted lysis while ensuring its activity at the pathogen–host interface.

phospholipase | activation | deoligomerization | membrane association | nicotinamide dinucleotide

Phospholipases are important enzymes in infectious disease pathogenesis involved in host modulation and damage. For example, some bacterial phospholipases, such as *Pseudomonas aeruginosa* ExoU, massively damage cells and contribute to host inflammatory response (1–4). Others, such as *Legionella pneumophila* VipD, facilitate bacterial intracellular replication by inhibiting phagosomal maturation, or as in the case of *Listeria monocytogenes*, phospholipases PlcA and PlcB are required for bacterial escape from the enclosing vacuole and for cell-to-cell spread (1, 5–8). Phospholipases have been assigned to different groups depending on the preferred cleavage site within their substrates. Phospholipases A (PLAs) and lysophospholipases A (LPLA) hydrolyze carboxyl ester bonds at the sn-1 or sn-2 position in phospholipids or lysophospholipids, respectively, and release fatty acids (1, 9). In *L. pneumophila*, a Gram-negative bacterium that causes Legionnaires' disease, at least 15 genes encoding PLAs/LPLAs belonging to three families are found. Many of these are secreted to modulate the host cell but only one, PlaB, is uniquely presented at the bacterial surface (1, 10–13).

In this study, we focused on PlaB, a hemolysin and virulence factor that promotes intracellular replication in macrophages by its PLA and LPLA activities (14–16). PlaB is also crucial for lung colonization and tissue destruction in guinea pig infections (13). It

is the only characterized member of a recently discovered PLA family, and homologs are found in a wide array of mostly water-associated bacteria including the opportunistic pathogen *P. aeruginosa* (14, 15). Previous work suggested that PlaB is organized into two domains, namely an N-terminal phospholipase (amino acids 1 to ~300) connected to a C-terminal domain (CTD) (amino acids ~301 to 474) that is also essential for activity (15). The catalytic triad S85/D203/H251 of the N-terminal domain (NTD) of PlaB and its homologs is embedded in uncommon consensus motifs which are unique among lipases (15). The CTD is not related to formerly characterized proteins, but we have earlier shown that the last 15 amino acids of PlaB are necessary for activity, although their exact role is not understood (15, 16). Subcellular fractionation and proteinase K digests revealed that PlaB is associated with the outer membrane (OM) and exposed on the surface. However, due to the apparent lack of export signal sequences, lipid anchors, or transmembrane helices, determinants for export and membrane association have not yet been characterized and therefore still remain elusive (13, 14).

PlaB represents a highly active PLA/LPLA of *L. pneumophila* and hydrolyzes lipids, such as phosphatidylcholine (PC) and phosphatidylglycerol (PG) found in the lung of the human host and in *Legionella* (14, 17–19). Hence, we reasoned that a control

## Significance

Secreted bacterial phospholipases, which hydrolyze host membranes, may also harm the pathogen itself. Sophisticated activation mechanisms are therefore required to prevent self-damage before protein export but warrant activity at the pathogen–host interface. Here we structurally analyzed PlaB, a surface-exposed highly active phospholipase and virulence factor of the lung pathogen *Legionella pneumophila*. Unexpectedly, we found that NAD(H), a central cofactor of energy metabolism, stabilizes an inactive tetrameric form of PlaB. Since NAD(H) is confined to the intracellular milieu of the bacterium, we propose that this sophisticated NAD(H)-dependent oligomerization mechanism protects *L. pneumophila* from damage and simultaneously enables the function of PlaB as a virulence factor after export and association to the bacterial surface.

Author contributions: M.D., W.M., P.A., W.B., and A.F. designed research; M.D., W.M., K.K.-K., S.W., and C.L. performed research; M.D., W.M., P.A., K.K.-K., J.P., J.K., S.W., C.L., W.B., and A.F. analyzed data; and M.D., W.M., W.B., and A.F. wrote the paper.

The authors declare no competing interest.

This article is a PNAS Direct Submission.

Published under the PNAS license.

<sup>1</sup>M.D. and W.M. contributed equally to this work.

<sup>2</sup>W.B. and A.F. contributed equally to this work.

<sup>3</sup>To whom correspondence may be addressed. Email: wulf.blankenfeldt@helmholtz-hzi.de or fliegera@rki.de.

This article contains supporting information online at <https://www.pnas.org/lookup/suppl/doi:10.1073/pnas.2017046118/-DCSupplemental>.

Published May 31, 2021.

mechanism of enzyme activity may be crucial to prevent damage to the pathogen itself. Indeed, PlaB shows an extraordinary activation mechanism that requires protein deoligomerization. At higher PlaB concentrations, the enzyme occurs in an inactive tetrameric form, whereas it deoligomerizes in the lower nanomolar concentration range where it possesses its highest specific activity (16). However, the mechanism behind enzyme regulation and whether the resulting dimer or monomer represents the active form is not understood.

To decipher the molecular basis for PlaB's unusual activation and to gain insight on how it associates with the OM, we have

determined its crystal structure. This allowed us to identify important structural features and, interestingly, revealed an NAD(H)-mediated tetramerization mechanism that controls activity.

## Results

**PlaB Crystallizes as a Dimer of Dimers and a Hook Structure Is Required for Dimer Formation.** Since PlaB is a virulence factor that raises potential biosafety concerns when produced in a heterologous host, we employed the inactive D203N mutant in our extensive efforts to obtain high-quality crystals. Most crystals suffered from anisotropic diffraction and streaky, overlapping reflections. The

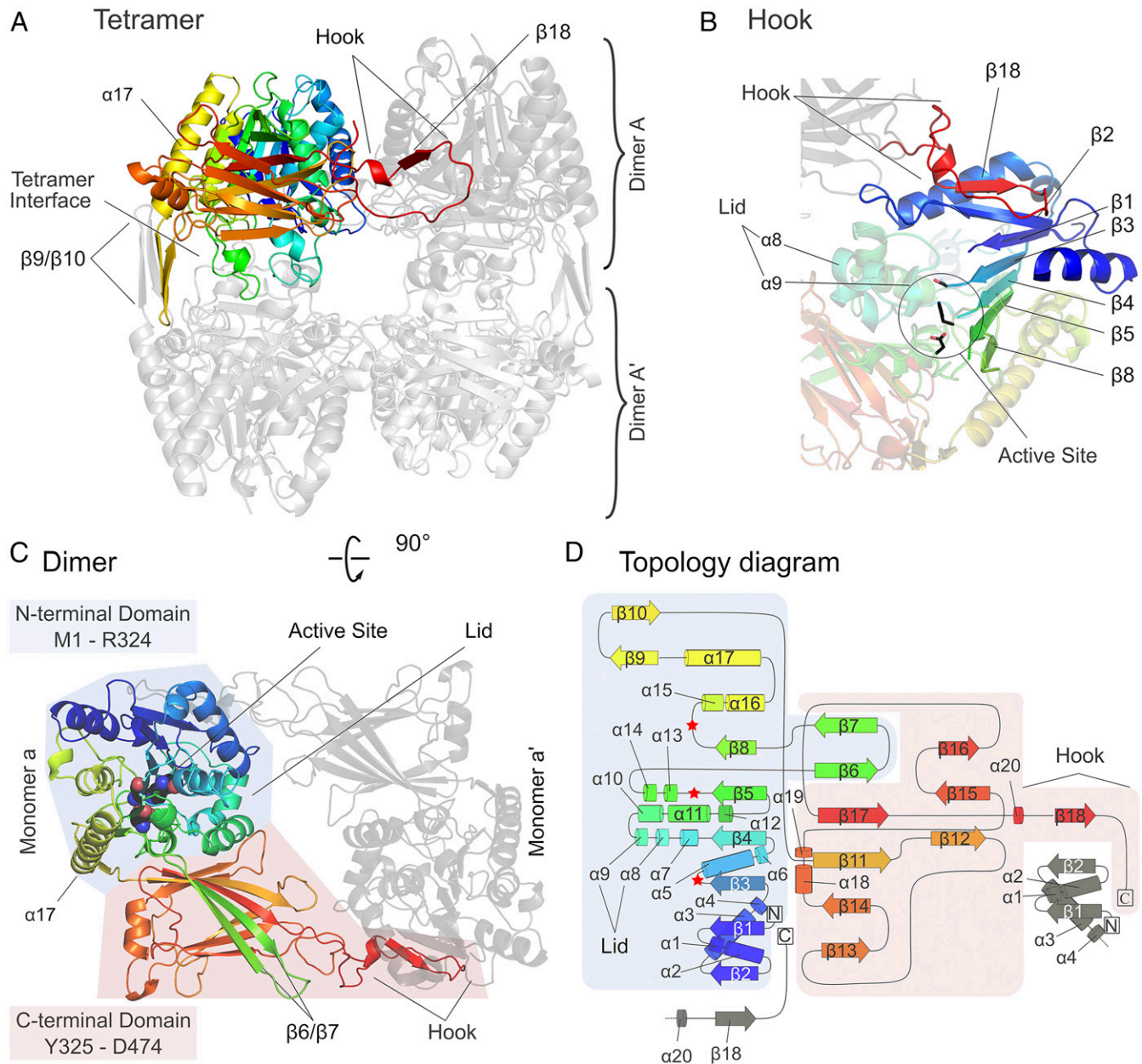


**Fig. 1.** PlaB crystallizes as a dimer of dimers, and a hook structure is required for dimer formation. (A) The PlaB tetramer is built from two identical dimers: dimer A (one monomer is shown with a rainbow color gradient, the other in dark gray) and dimer A' (lighter greys).  $\alpha$ -17 leads to  $\beta$ -9/ $\beta$ -10, which participate in the tetramer interface. The C terminus folds into a hook structure that connects the protomers of one PlaB dimer via head-to-tail interactions. (B)  $\beta$ -18 of the hook (shown in red) attaches to  $\beta$ -2 of the second protomer in the dimer. The active site is covered by a lid in the closed conformation ( $\alpha$ -8/ $\alpha$ -9). (C) PlaB consists of an N-terminal phospholipase domain (NTD, blue background) with a typical but extended  $\alpha/\beta$ -hydrolase fold and a C-terminal bilobed  $\beta$ -sandwich domain (CTD, red background).  $\beta$ -6/ $\beta$ -7 (green) protrude from the NTD into the CTD. (D) Topology diagram of PlaB. The same color schemes as in A and C have been used.

structure was finally determined at 2.3-Å resolution by single-wavelength anomalous dispersion of seleno-*L*-methionine-labeled PlaB in a crystal obtained by seeding (*SI Appendix*, Fig. S1 *A* and *B*). This crystal belonged to space group  $P2_1$  and displayed strong translational noncrystallographic symmetry, explaining why the refinement converged at very high R-factors for this data set (*SI Appendix*, Table S1). The asymmetric unit comprised four chains that arrange in a tetrameric fashion, best described as a dimer of dimers (Fig. 1*A*). Interestingly, the interface between both dimers is relatively small, and PISA analysis of the protein chains alone did not recognize this tetramer as a stable assembly (20). The PlaB dimers, however, are predicted as stabilized by approximately -29.8 kcal/mol, suggesting that they represent the active form of PlaB. The dimers are formed by head-to-tail interaction between the N-terminal phospholipase domain of the first monomer and a protruding hook-like extension at the C terminus of the second monomer (residues R446 to D474) (Fig. 1 *A–C* and *SI Appendix*, Table S2). This leads 1) to structural complementation of the central  $\beta$ -sheet of the phospholipase domain by  $\beta$ -18 from the hook region (see Fig. 3*B*), explaining the previously determined loss of activity when residues from the C terminus are deleted (15, 16), and 2) to a number of polar and hydrophobic interchain interactions between the last ~30 amino acids and residues of the N terminus.

**The N-Terminal Phospholipase Domain Is a Typical  $\alpha/\beta$ -Hydrolase Extended by the Noncanonical Two-Stranded  $\beta$ -Sheets  $\beta$ -6/ $\beta$ -7 and  $\beta$ -9/ $\beta$ -10.** The PlaB monomer consists of two clearly distinguishable domains (Fig. 1 *C* and *D* and *SI Appendix*, Fig. S2). These comprise residues 1 to ~324 and residues ~325 to 474, representing the N-terminal phospholipase domain and a CTD consisting of a bilobed  $\beta$ -sandwich extended by the hook structure, respectively. The NTD displays a typical  $\alpha/\beta$ -hydrolase (ABH) fold, hallmarked by a central six-stranded parallel  $\beta$ -sheet (spatially ordered as  $\beta$ -2,  $\beta$ -1,  $\beta$ -3,  $\beta$ -4,  $\beta$ -5,  $\beta$ -8) surrounded by 17  $\alpha$ -helices ( $\alpha$ -1 to  $\alpha$ -17) (Fig. 1 *A*, *C*, and *D*) (21, 22). The catalytic center is readily discernible by the catalytic triad S85/D203/H251 that has previously been identified through sequence alignments and mutagenesis (Fig. 1 *B* and *C*) (15). It is shielded from the solvent by a closed lid formed by residues G127 to G144 of  $\alpha$ -8 and  $\alpha$ -9, as is frequently observed in ABHs in the absence of substrates (Fig. 1 *B* and *C* and *SI Appendix*, Table S2) (23). The quality of the electron density indicates that this lid is highly flexible. In addition to these canonical features, the NTD also possesses unique structural elements that are specific to PlaB, namely a long  $\alpha$ -helix ( $\alpha$ -17, residues R285 to N305) and two antiparallel  $\beta$ -sheets ( $\beta$ -6/ $\beta$ -7, residues S216 to R237 and  $\beta$ -9/ $\beta$ -10, residues K308 to I321) (Fig. 1 *A*, *C*, and *D* and *SI Appendix*, Table S2). While the  $\alpha$ -helix participates in lining the large central  $\beta$ -sheet, the additional  $\beta$ -sheets  $\beta$ -6/ $\beta$ -7 and  $\beta$ -9/ $\beta$ -10 protrude from the ABH fold (Fig. 1 *A* and *C* and *SI Appendix*, Fig. S2).

**The C-Terminal Domain Possesses a Mosaic Bilobed  $\beta$ -Sandwich Structure.** The CTD of PlaB is dominated by a bilobed  $\beta$ -sandwich consisting of a six-stranded mixed ( $\beta$ -6,  $\beta$ -7,  $\beta$ -11,  $\beta$ -13,  $\beta$ -14, and  $\beta$ -17) and a three-stranded antiparallel  $\beta$ -sheet ( $\beta$ -12,  $\beta$ -15, and  $\beta$ -16) (Fig. 1 *C* and *D* and *SI Appendix*, Fig. S3). Interestingly, two strands of the first  $\beta$ -sheet stem from the NTD ( $\beta$ -6 and  $\beta$ -7) (Fig. 1 *C* and *D*). Searches with DALI (24) reveal similarity to immunoglobulin-like domains; however, none of the identified structures possesses the mosaic nature and the ensuing  $\beta$ -sheet extension by  $\beta$ -6/ $\beta$ -7, suggesting that the CTD of PlaB represents a not previously observed fold (*SI Appendix*, Fig. S3).

**PlaB Shows a Broad Substrate Spectrum, and Mutations in the Lid or  $\beta$ -9/ $\beta$ -10 Alter Substrate Specificity.** PlaB hydrolyzed a broad array of biologically important phospholipids and lysophospholipids. Activity was found toward negatively charged substrates such as PG, phosphatidylserine, phosphatidylinositol (PI), and also toward

PC, which contains a positively charged head group (Fig. 2*A*). With respect to PI, different derivatives were hydrolyzed (*SI Appendix*, Fig. S4). PIs are pivotal constituents of the LCV that impact on its membrane dynamics and on vesicle trafficking. *L. pneumophila* modifies these compounds to its own advantage during host infection (25). To gain insight into determinants for activity and this substrate spectrum, we analyzed the importance of certain structural elements, specifically the lid, the hook,  $\beta$ -6/ $\beta$ -7, and  $\beta$ -9/ $\beta$ -10. A lid is a typical feature of lipases regulating substrate access to the catalytic site. Both its amphipathic nature and specific amino acids are crucial for activity and specificity (23, 26). Indeed, we found that the lid point mutation S129A had severely reduced activity toward PC but only slightly reduced activity toward PG and lysophosphatidylglycerol (LPG) (Fig. 2 *B–D*). This is in accordance with previous findings showing that this residue, now recognized as part of the lid, promotes PC hydrolysis and hemolysis (15). Furthermore, the positive charge of the neighboring lid residues R130 and R133 could contribute to the recognition of negatively charged lipid substrates, as has been observed for other lid-containing hydrolases (21, 23). Indeed, whereas point mutations led to reduced activity toward PG and LPG but also influenced PC hydrolysis, the triple mutant S129A/R130A/R133A was inactive toward all substrates tested (Fig. 2*D*). These findings demonstrate that the lid region influences activity and substrate specificity.

The noncanonical  $\beta$ -strands  $\beta$ -6/ $\beta$ -7 and  $\beta$ -9/ $\beta$ -10 are antiparallel to each other and project away from the ABH fold (Fig. 1 *A* and *C* and *SI Appendix*, Fig. S2). Given the importance of strands  $\beta$ -6 and  $\beta$ -7 within the structure of the CTD (*SI Appendix*, Fig. S3), it is not surprising that the respective deletion mutant was inactive (*SI Appendix*, Fig. S5 *A* and *B*). A similar phenotype was found when the hook (residues R446 to D474) was deleted (*SI Appendix*, Fig. S5 *A* and *B*). This is in accordance with previous observations where shortening of the CTD led to a decrease in activity (16), corroborating our finding that the hook connects two PlaB monomers and extends the ABH fold to yield active PlaB dimers. The  $\Delta\beta$ -9/ $\beta$ -10 mutant lost its activity against PC but retained a lower level of activity toward PG and LPG. Therefore,  $\beta$ -9/ $\beta$ -10 affects the substrate spectrum of PlaB (Fig. 2 *E* and *F*). An intriguing pattern of hydrophobic and cationic residues displayed on both sides of the  $\beta$ -9/ $\beta$ -10 sheet (K308, F310, K312, F316, R318, and Y320) resembles motifs known to contribute to cation- $\pi$  interactions in proteins that bind to positively charged phospholipid head groups (Fig. 2*E*) (27, 28). Consistently, the corresponding triple mutant F310D/F316D/Y320D indeed resembled the  $\Delta\beta$ -9/ $\beta$ -10 mutant in terms of activity (Fig. 2 *E* and *F*).

**$\beta$ -9/ $\beta$ -10 Contributes to Tetramer Stability, Membrane Binding, OM Localization of PlaB, and Bacterial Integrity.** The position of sheet  $\beta$ -9/ $\beta$ -10 in the tetramer suggests that it may be involved in dimer/dimer interactions (Fig. 1*A*) and indeed, as size-exclusion chromatography-multiangle light scattering (SEC-MALS) experiments showed, deletion or mutation impeded concentration-dependent tetramerization. Specifically, whereas different concentrations of PlaB wildtype (WT) revealed either the tetramer only or a tetramer-dimer mixture, the  $\Delta\beta$ -9/ $\beta$ -10 or F310D/F316D/Y320D mutants were present in a dimeric form regardless of protein concentration (Fig. 3*A* and *SI Appendix*, Table S3). Together, these data establish that  $\beta$ -9/ $\beta$ -10 not only tunes selectivity of PlaB toward PC but also contributes to stabilization of the tetrameric state.

Furthermore, because of its exposed location, it is conceivable that, when the tetramer deoligomerizes to active dimers, sheet  $\beta$ -9/ $\beta$ -10 is liberated and may subsequently be involved in OM association. We therefore investigated association of PlaB and the  $\Delta\beta$ -9/ $\beta$ -10 mutant to PG and PC liposomes since PG and PC are major constituents of the *L. pneumophila* OM (29). We found that higher amounts of  $\Delta\beta$ -9/ $\beta$ -10 than of PlaB WT remained in the supernatant, suggesting that it associated less efficiently to the

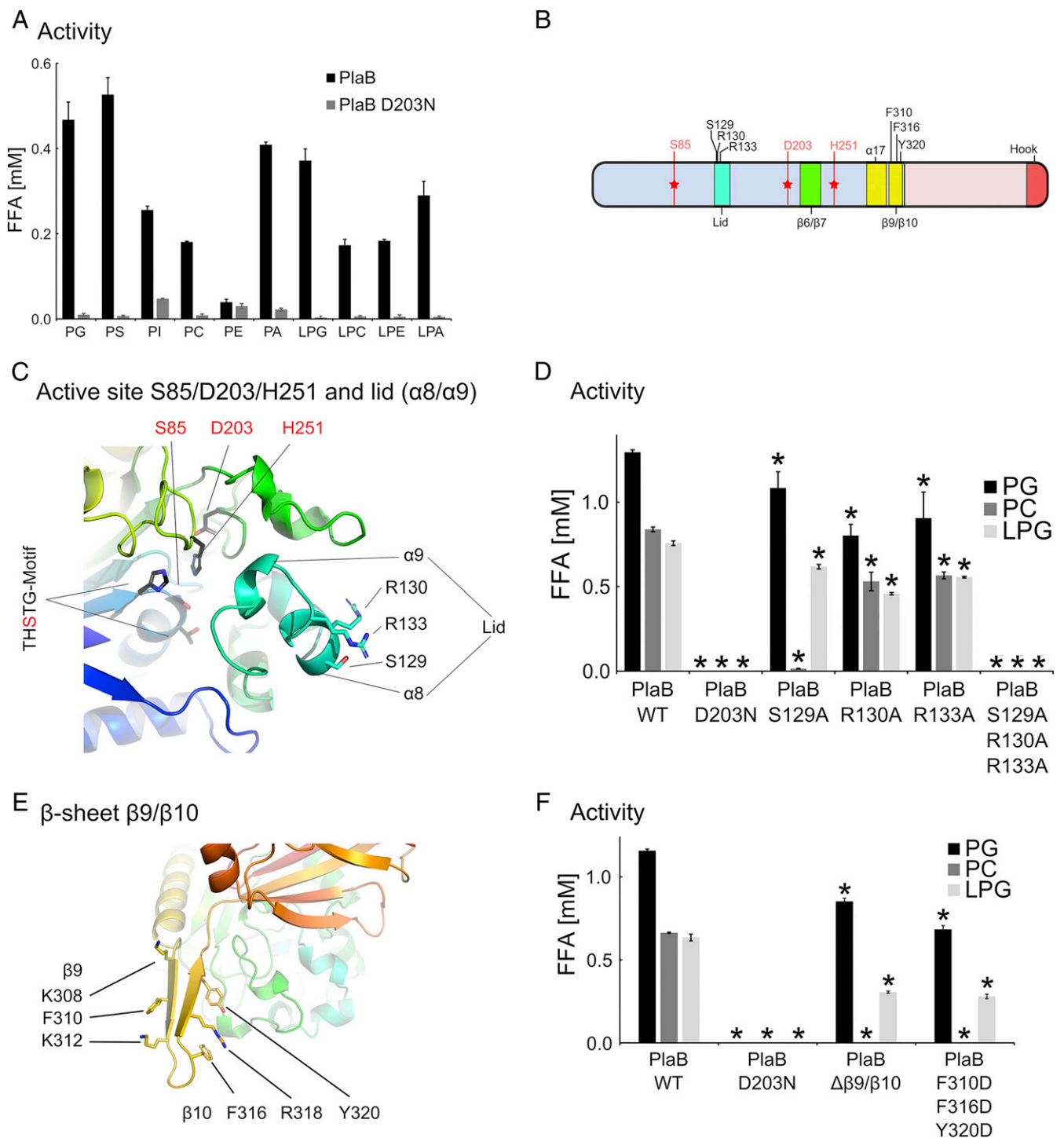


**Fig. 2.** PlaB shows a broad substrate spectrum, and mutations in the lid or  $\beta$ -9/ $\beta$ -10 alter substrate specificity. (A) Enzymatic activity of PlaB WT and the catalytic mutant D203N toward different lipid substrates. A total of 0.233-nM protein was incubated with 0.5 mM of the indicated lipids for 60 min before released fatty acids (FFA) were quantified. The error bars indicate SD of three independent measurements. Abbreviations: PG, phosphatidylglycerol; PS, phosphatidylserine; PI, phosphatidylinositol; PC, phosphatidylcholine; PE, phosphatidylethanolamine; PA, phosphatidic acid; LPG, lysophosphatidylglycerol; LPC, lysophosphatidylcholine; LPE, lysophosphatidylethanolamine; and LPA, lysophosphatidic acid. (B) Overview of PlaB sequence and structural features, such as the active site (red stars). The position of residues mutated in the experiments shown in this figure are indicated. (C) Active site (S85/D203/H251) and lid ( $\alpha$ -8/ $\alpha$ -9, cyan) in their structural context. S85 is embedded in the THSTG motif. (D) Enzymatic activity of PlaB WT and mutants (D203N, S129A, R130A, R133A, and S129A/R130A/R133A) toward different phospholipids. A total of 1:100 diluted cell lysates of *E. coli* expressing different PlaB versions were incubated with lipids (1 mM) for 15 min and FFA were quantified. The error bars indicate SDs of three independent measurements. Statistical analysis was performed using two-tailed, unpaired Student's *t* tests, relating PlaB WT to PlaB versions.  $*P < 0.02$  ( $n = 3$ ). Western blot of cell lysates or SDS-PAGE analysis of proteins (*SI Appendix, Fig. S6*). (E)  $\beta$ -9/ $\beta$ -10 (yellow) protrudes from the NTD and is decorated with cationic and aromatic residues, of which some were probed by mutagenesis as shown in F. (F) Enzymatic activity of PlaB WT and mutants (D203N,  $\Delta\beta$ -9/ $\beta$ -10, and F310D/F316D/Y320D) toward different phospholipids (1 mM). A 0.233-nM protein was incubated with the indicated lipids for 30 min and FFA were quantified. The error bars indicate SDs of three independent measurements. Statistical analysis was performed using two-tailed, unpaired Student's *t* tests, relating PlaB WT to PlaB versions.  $*P < 0.02$  ( $n = 3$ ). Western blot of cell lysates or SDS-PAGE analysis of proteins (*SI Appendix, Fig. S6*).

liposomes (Fig. 3B). Similar results were observed upon addition of the proteins to the *L. pneumophila*  $\Delta$ plaB mutant. Specifically, higher amounts of  $\Delta\beta$ -9/ $\beta$ -10 were present in the supernatant and accordingly lower amounts associated with the bacteria (Fig. 3C). This indicates that  $\beta$ -9/ $\beta$ -10 is an important element acting as membrane attachment structure, a fact which might additionally contribute to efficient phospholipid hydrolysis (Fig. 2F).

Next, we were interested if OM localization of PlaB was affected by deletion of  $\beta$ -9/ $\beta$ -10. We first confirmed membrane, OM, and surface localization of PlaB WT in *L. pneumophila* by means of 1) subcellular fractionation (SI Appendix, Fig. S7A and B), 2) proteinase K digestion (SI Appendix, Fig. S7C), and 3) surface-protein biotin labeling (SI Appendix, Fig. S7D). Since the export mechanism of PlaB in *L. pneumophila* is unclear and did not involve several *Legionella*-specific secretion systems (13), we tested if it is exported in *Escherichia coli*. In addition, implementation of *E. coli* as a model system would further allow the analysis of PlaB variants released from the membrane in the absence of potentially PlaB-degrading enzymes, such as the *L. pneumophila* zinc metalloproteinase ProA (30). We indeed found that PlaB and the catalytic mutant D203N localized to the OM (Fig. 3D and SI Appendix, Fig. S8). However, the  $\Delta\beta$ -9/ $\beta$ -10 and the F310D/F316D/Y320D mutants showed subcellular mislocalization, specifically a main protein fraction associated with the inner membrane (Fig. 3D and SI Appendix, Fig. S9). All other mutants in the lid, hook, or  $\beta$ -6/ $\beta$ -7 localized to the OM similar to the WT protein (SI Appendix, Figs. S8 and S10). In addition,  $\Delta\beta$ -9/ $\beta$ -10 was released into the culture supernatant, unlike intact PlaB (Fig. 3E). To further substantiate our findings, we expressed truncations of PlaB in *L. pneumophila* and analyzed surface presentation by means of proteinase K digests, which again corroborated the importance of  $\beta$ -9/ $\beta$ -10 (SI Appendix, Fig. S11). In summary, the  $\Delta\beta$ -9/ $\beta$ -10 protein was malfunctioning in terms of tetramer stabilization and in OM association. Since these two aspects are important for control and localization of PlaB activity,  $\Delta\beta$ -9/ $\beta$ -10 may have detrimental effects for the bacteria. Indeed, a *L. pneumophila*  $\Delta$ proA strain expressing  $\Delta\beta$ -9/ $\beta$ -10 released isocitrate dehydrogenase (ICDH), a cytosolic marker, but not a strain with WT PlaB (Fig. 3F). Furthermore, a reduction of  $\Delta\beta$ -9/ $\beta$ -10 in the cell pellet was observed at higher ODs, indicating membrane release of the variant. However,  $\Delta\beta$ -9/ $\beta$ -10 was not detected in the culture supernatant likely because of proteolytic degradation by enzymes other than ProA. In conclusion, this confirms the key importance of the  $\beta$ -9/ $\beta$ -10 structural element in functional and spacial control of *L. pneumophila* PlaB.

**PlaB Phospholipase Activity Is Controlled by NAD(H)-Mediated Tetramerization.** The fact that the tetramer is not recognized as a stable entity in structure-based calculations with PISA yet is a dominant species in experiments raises the question how it may be stabilized in solution. While tetramer formation was found to be concentration dependent, we were surprised to observe copurified ligands at the dimer/dimer interface, albeit at low occupancy in the initial crystal structure. The shape of the electron density suggested the identity of these ligands as NAD(H) molecules that bind to two different but closely neighbored binding sites per monomer (Fig. 4A and B). Tetramers were the only species found to bind NADH here. In detail, we observed that 1) the presence of NAD(H) in the SEC-MALS running buffer led to the exclusive formation of tetramers (Fig. 4C), 2) in freshly purified PlaB, the A260/A280 ratio in the SEC-MALS experiment was higher than expected for the peak corresponding to tetrameric PlaB but not for lower oligomers (SI Appendix, Fig. S12), 3) the addition of NAD(H) led to a more defined melting point (SI Appendix, Fig. S13), and 4) thio-NAD (SNAD), a component of the thermal shift assay (TSA) used to optimize the storage buffer for PlaB, improved and accelerated crystallization of the PlaB tetramer, yielding crystals in spacegroup P1 that diffracted up to 1.8 Å and that grew to full size after 20 instead of 150 d (SI Appendix, Fig.

S1C). The corresponding structure indeed revealed full occupation of the eight NAD(H) binding sites with SNAD molecules (Fig. 4A and SI Appendix, Fig. S14). The binding sites seem to be accessible through large channels in the dimer/dimer interface (SI Appendix, Fig. S15), and several residues are involved in specific interactions with the ligand, particularly from the NTD ( $\beta$ -9/ $\beta$ -10,  $\alpha$ -13, and lid) of one PlaB dimer and from the CTD ( $\beta$ -12,  $\beta$ -13, and  $\beta$ -14) of the other, also including  $\pi$ -stacking between the nicotinamide group and Y190 and Y196 (Fig. 4B). Interestingly, while all eight NAD(H) binding sites are occupied with SNAD, a substantial part of the lid of all four monomers became extremely flexible such that residues 133 to 141 (RIKSFFEGI) could not be traced in the corresponding structure. The noncanonical strands  $\beta$ -9/ $\beta$ -10 of one dimer line the outer NAD(H) binding site, and R318 is involved in a hydrogen bond with the ribose unit of the nicotinamide half of the ligand (Fig. 4B and SI Appendix, Fig. S14).

When we reanalyzed the crystal structure of PlaB in the ligand-bound form with PISA, we found that the tetramer was calculated to be strongly stabilized by SNAD ( $\Delta G = -44.7$  kcal/mol with SNAD and  $-3.0$  kcal/mol without SNAD) (20). This suggests that tetramerization and hence inactivation of PlaB is NAD(H) mediated. Consistently, we confirmed that NAD<sup>+</sup> and NADH inhibited the activity of WT PlaB (Fig. 4D). Although residues of  $\beta$ -9/ $\beta$ -10 among others were found in close proximity to the ligand, the activity of the  $\Delta\beta$ -9/ $\beta$ -10 and the F310D/F316D/Y320D mutant was also reduced by NAD(H), demonstrating the importance of additional NAD(H) interaction sites (Fig. 4A, B, and D). Furthermore, it was possible to reconstitute tetramers for all concentrations of the WT and mutant proteins when NAD(H) was added (Fig. 4C). This shows that the tetrameric form of the mutants, although less stable without ligand addition (Fig. 3A), was stabilized by the ligand (Fig. 4C). We conclude that NAD(H) enhances PlaB tetramerization and concomitantly enzyme inactivity, establishing an allosteric regulatory process.

We used the crystal structure to design mutants that should have impaired NAD(H) binding. We mutated R130, R366, and Y378 that tightly interact with NAD(H) in one or both binding sites and combined these with each other or with  $\Delta\beta$ -9/ $\beta$ -10. However, combined mutants lost activity and single mutants which retained at least partial activity still responded to NAD(H) (SI Appendix, Fig. S16). This led us to the conclusion that deletion of NAD(H) binding sites will also impair activity.

**PlaB Is Widely Distributed in Several Bacterial Phyla.** A BLAST search revealed high conservation of PlaB in the *Legionella* genus, mostly showing over 80% protein identity with the exception of about one-third of the non-*pneumophila* species (SI Appendix, Fig. S17) (31). PlaB-like proteins were further found in a variety of genera of several bacterial phyla. Using the UniRef90 database (32), we constructed a sequence similarity network of about 200 PlaB-like proteins by defining clusters of 50% sequence identity (SI Appendix, Fig. S18) (33). Alignment of representatives of these clusters revealed that the two-domain structure of PlaB seems preserved. The  $\beta$ -9/ $\beta$ -10 element and NAD(H)-interacting residues were less conserved (SI Appendix, Fig. S19). We conclude that PlaB is widely distributed in bacteria and that residues for NAD(H) interaction and OM association via  $\beta$ -9/ $\beta$ -10 are highly conserved in many *Legionella* species, suggesting a similar control mechanism which may further be relevant in some other bacteria.

## Discussion

Here we determined the crystal structure of *L. pneumophila* PlaB, demonstrating that the intrinsically unstable tetramer contains two stable dimers. PlaB consists of an ABH in its NTD (21), followed by a  $\beta$ -sandwich domain in the CTD that is completed by two noncanonical  $\beta$ -strands from the NTD ( $\beta$ -6/ $\beta$ -7). The other additional two-stranded  $\beta$ -sheet  $\beta$ -9/ $\beta$ -10 of the NTD fulfills several roles for the enzyme. Its deletion changed enzymatic activities,

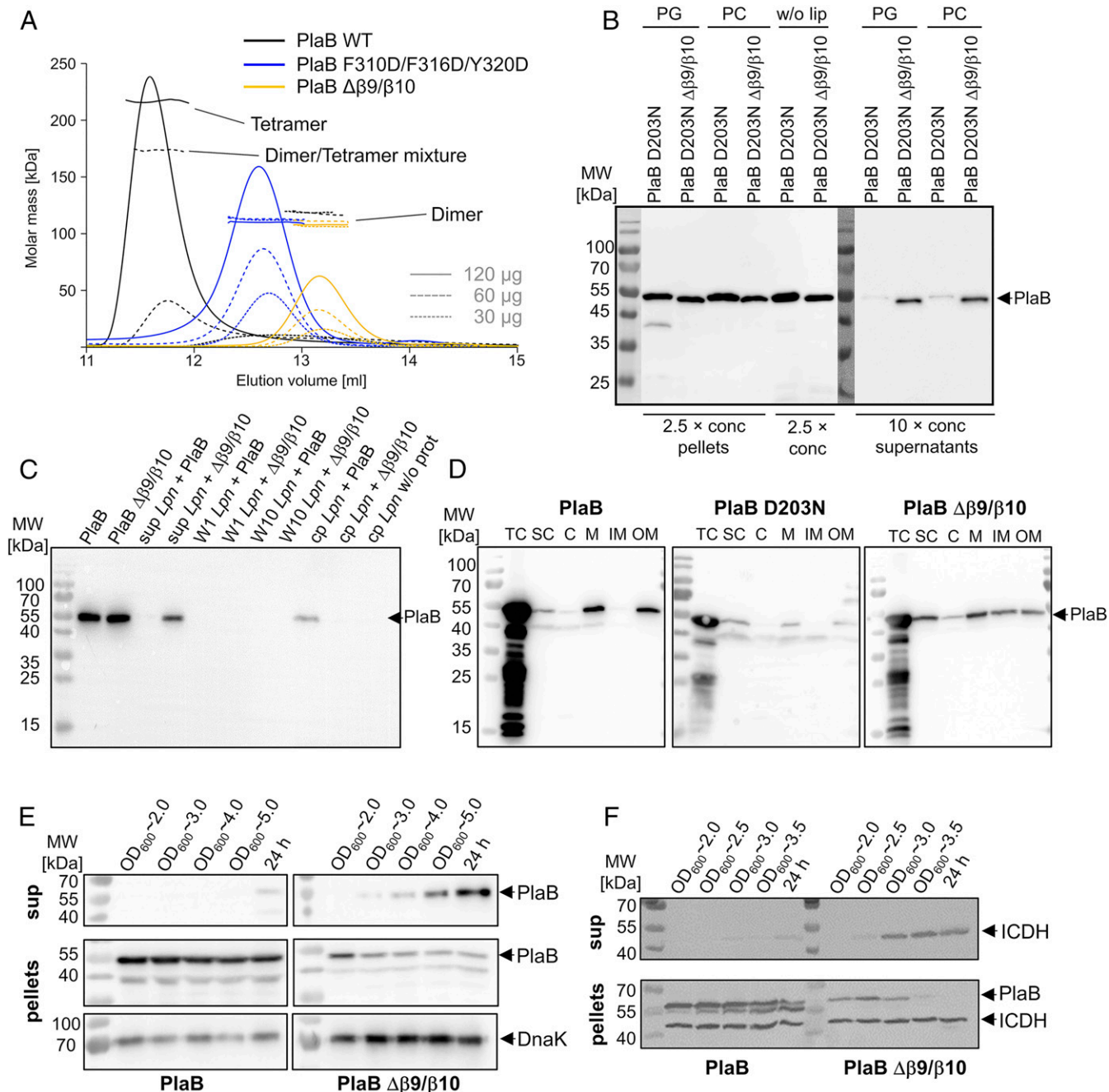
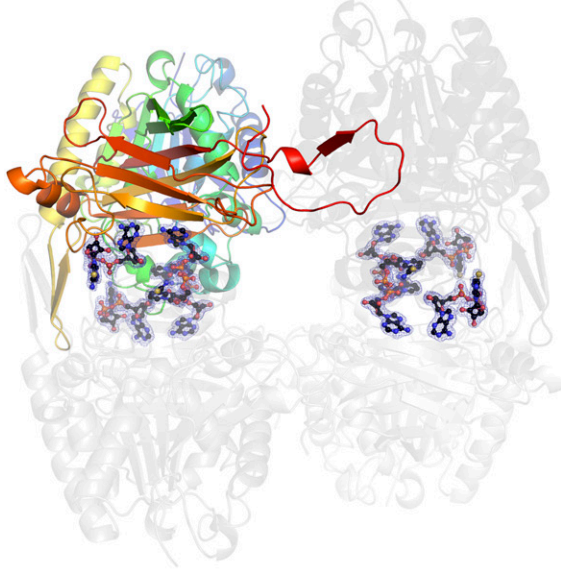
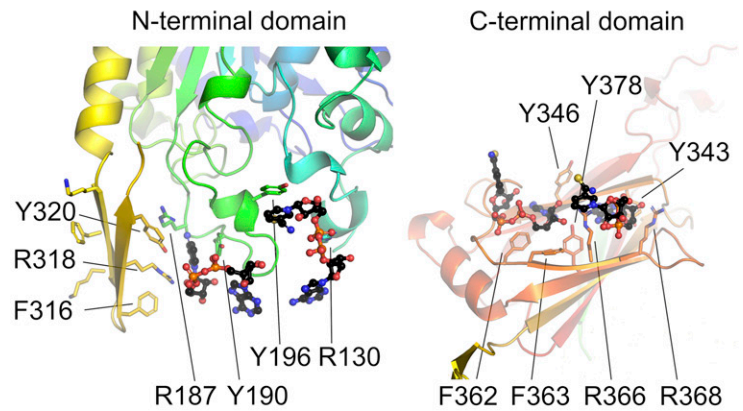


**Fig. 3.**  $\beta$ -9/ $\beta$ -10 contributes to tetramer stability, membrane binding, OM localization of PlaB, and bacterial integrity. (A) SEC-MALS analysis of PlaB WT (black),  $\Delta\beta$ -9/ $\beta$ -10 (yellow), and F310D/F316D/Y320D (blue). The amounts of protein applied were 120 (solid lines), 60 (longer dashes), or 30  $\mu\text{g}$  (short dashes), leading to tetramers, tetramer/dimer mixtures, or dimers as indicated. Detailed results are shown in *SI Appendix, Table S3*. (B) Liposome colocalization assay of PlaB D203N and D203N  $\Delta\beta$ -9/ $\beta$ -10 protein. Western blot analysis of pellets and supernatants after liposome incubation with 0.3- $\mu\text{M}$  PlaB versions for 30 min and ultracentrifugation using anti-strep-tag antibody. (C) External association of different PlaB versions to *L. pneumophila*. Western blot of supernatants (sup), washing fractions (W1 and W10), and cell pellets (cp) using strep-tag antibody after incubation of *L. pneumophila*  $\Delta\text{plaB}$  with 0.3- $\mu\text{M}$  PlaB versions for 10 min, 10 washing steps, and cell lysis. (D) Localization of different PlaB versions. Western blot analysis after cell fractionation of *E. coli* expressing different PlaB versions using an anti-strep-tag antibody. Please refer to *SI Appendix, Fig. S7–S9* for PlaB WT or mutant analysis including fractionation controls. Abbreviations: TC, total cell lysate; SC, soluble content; C, cytosol; M, membrane; IM, inner membrane; and OM, outer membrane. (E) Detection of PlaB localization during growth in *E. coli*. Western blot analysis for detection of PlaB (anti-strep-tag antibody) and the cytosolic control protein DnaK (anti-DnaK antibody) in cell lysates and culture supernatants of *E. coli* expressing *plaB* WT or  $\Delta\beta$ -9/ $\beta$ -10. (F) Detection of PlaB localization and bacterial lysis during growth in *L. pneumophila*. Western blot analysis of cell lysates and culture supernatants of *L. pneumophila*  $\Delta\text{proA}$  expressing *plaB* WT and  $\Delta\beta$ -9/ $\beta$ -10. 4 $\times$ HA-PlaB and the cytosolic control protein ICDH were detected by using an anti-HA.11 epitope tag antibody and an ICDH antibody.

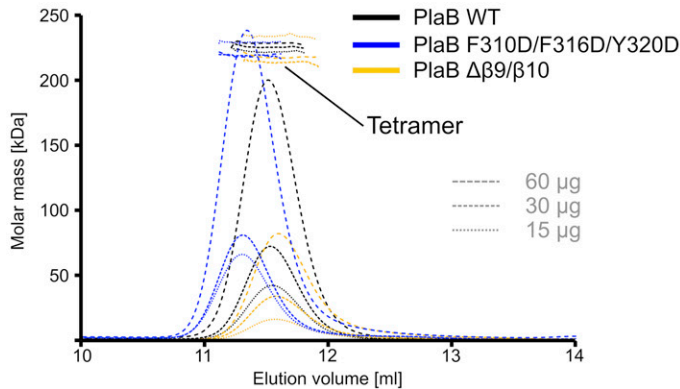
### A SNAD in PlaB tetramer



### B SNAD interactions



### C Oligomerization / Influence of NAD<sup>+</sup>



### D Activity / Influence of NAD<sup>+</sup>/NADH

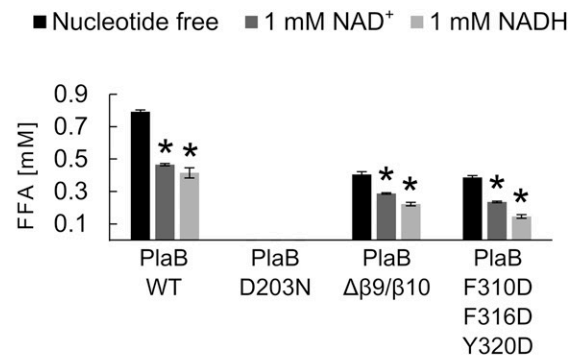


**Fig. 4.** PlaB phospholipase activity is inhibited by NAD(H)-mediated tetramerization. (A) The position of eight NAD(H) binding sites within the PlaB tetramer, shown in the same orientation as in Fig. 1A. Note that the identity of these ligands is the thio-derivative SNAD, since the respective data were obtained from a crystal generated in the presence of 1 mM SNAD (*SI Appendix, Fig. S1C*). The blue mesh indicates the final  $|2F_o - F_c|$  electron density for the ligands, displayed at  $1 \sigma$ . (B) Two SNAD molecules per PlaB monomer are coordinated at the tetramer interface. The NTD (*Left*) contributes with  $\beta$ -9/ $\beta$ -10 (yellow),  $\alpha$ -13 (green), and the lid structures (cyan), the CTD (*Right*) with  $\beta$ -12,  $\beta$ -13, and  $\beta$ -14 (orange) to SNAD coordination. (C) SEC-MALS analysis of PlaB and  $\beta$ -9/ $\beta$ -10 mutants in the presence of 1 mM NAD<sup>+</sup> shows tetramers regardless of protein concentration and version (PlaB WT [black],  $\Delta\beta$ -9/ $\beta$ -10 [yellow], and F310D/F316D/Y320D [blue]). The amounts of protein applied were 60 (longer dashes), 30 (shorter dashes), or 15  $\mu$ g (dots). Detailed results are shown in *SI Appendix, Table S3*. (D) Enzymatic activity of PlaB WT and mutant strains (D203N,  $\Delta\beta$ -9/ $\beta$ -10, and F310D/F316D/Y320D) toward PG with/without NAD<sup>+</sup> or NADH addition. A 0.233-nM protein was incubated with PG (1 mM) for 30 min and released fatty acids were quantified. The error bars indicate SDs of three independent measurements. Statistical analysis was performed using two-tailed, unpaired Student's *t* tests, relating PlaB versions without nucleotides to PlaB versions supplemented with NAD(H). \**P* < 0.02 (*n* = 3). SDS-PAGE analysis of proteins (*SI Appendix, Fig. S6*).

tetramer stability, membrane binding, as well as localization to the OM, and as a consequence the lack threatens bacterial integrity. Some of these traits seem to be rooted in patterns of cationic and aromatic amino acids that protrude from  $\beta$ -9/ $\beta$ -10 and are known to promote phospholipid interaction by means of cation- $\pi$  interactions (27, 28). The finding of a C-terminal hook-like structure that connects two monomers and contributes a strand to the central ABH  $\beta$ -sheet was unprecedented but explains the importance of C-terminal residues for enzyme activity (16). Similar to many ABH enzymes studied in the absence of substrate (34), tetrameric PlaB contains a flexible lid adopting a closed conformation. Tetramerization sequesters the lids of all four PlaB molecules at the tetramer interface, thereby hampering their interaction with phospholipids and explaining the inactivity of the tetrameric form. The most unexpected finding was the observation

of eight NAD(H) molecules specifically bound to the dimer/dimer interface of the tetramer. Our experiments revealed the importance of NAD(H) for the stability of the tetramer and hence enzyme inhibition. Binding of NAD(H) likely involves residues from several structural elements, including the lid. Thus, NAD(H) may contribute to lid immobilization in the closed state. It is therefore hypothesized that the lid is only able to open when PlaB is present as a dimer and comes into contact with the substrate (23, 34). In other ABHs, the lid impacts substrate specificity (26), as also found here and before for residue S129, determining PC specificity (15).

NAD(H) appears to be a particularly attractive compound for controlling the activity of PlaB, since it is a central cofactor in energy homeostasis (35) expected to be confined to the intracellular milieu. Both the oxidized form NAD<sup>+</sup> and the reduced form NADH inhibited PlaB. NAD<sup>+</sup> is usually present in much higher

amounts than NADH, and intracellular concentrations of NAD<sup>+</sup> reach millimolar levels (36, 37), implying that NAD<sup>+</sup> might have a greater impact on PlaB regulation.

We therefore prefer the following model of PlaB activation and localization control: high concentrations of intracellular NAD(H) mediate tetramer formation of PlaB and thus inhibit lipolytic activity and presumably protect bacteria from lysis. Once the enzyme is exported, the concentration of NAD(H) drops significantly, leading to the formation of active dimers. This may involve the initial dissociation of the dinucleotides through the large solvent-accessible channels in the dimer/dimer interface followed by separation of the tetramer or, vice versa, separation of the tetramer followed by dissociation of the dinucleotides in a second step. Regardless, dissociation of the tetramer will liberate β-9/β-10 from the dimer/dimer interface and thus transform the protein complex into its membrane-interacting form (Fig. 5). Disturbance of this process by deletion of β-9/β-10 affects tetramer stability and proper localization, which then leads to bacterial lysis.

Calculations show that NAD(H) stabilizes the PlaB tetramer by  $-44.7$  kcal/mol whereas the nucleotide-free tetramer is unstable. Each dimer, though, is stabilized by  $-29.8$  kcal/mol. In the dimeric form of PlaB, β-9/β-10 becomes accessible for membrane interaction. The expected energy gain upon membrane association of two PlaB dimers with two β-9/β-10 elements each can be estimated to amount to approximately  $-40$  kcal/mol (38), disregarding possible further energy gain due to interactions between the CTD and the membrane. Together, this hints at a fine-tuned regulatory mechanism linking ligand-dependent oligomerization, activity, and localization on the one hand for protection of *L. pneumophila* from PlaB-mediated self-lysis and on the other for presentation of the active enzyme at the host–pathogen interface. In this regard, it is interesting that membrane-associated PlaB cannot be released again by washing with NAD(H), which points at a tight membrane interaction once the enzyme has reached its destination (SI Appendix, Fig. S20).

Questions remain with respect to the exact role of PlaB at the OM in *Legionella* infections, and different functions can be envisioned. First, PlaB could promote intracellular replication by remodeling the LCV membrane to its own advantage [e.g., by cleaving PI derivatives and thereby impacting also on vesicular trafficking (25)]. Second, PlaB may contribute to the maintenance of bacterial OM asymmetry by hydrolyzing mislocalized phospholipids, similar to the enterobacterial phospholipase PldA (39–41). Even if PlaB, unlike PldA, is not an integral membrane protein, this could improve resistance to stressful conditions and therefore support intracellular propagation.

NAD(H) acts as a cofactor of enzymes in numerous fundamental cellular processes (42); yet cases where NAD(H) triggers inactivity by means of tetramerization such as in PlaB have to our knowledge not yet been described. Furthermore, several enzymes that require oligomerization to obtain full activity are known (43, 44), but the opposite (i.e., deoligomerization leading to activation) is rare (45, 46). Examples include the trimeric purine nucleoside phosphorylase from bovine spleen, which dissociates into significantly more active monomers upon dilution (47), or the dimeric *Crotalus atrox* venom PLA<sub>2</sub>, which seems to split into monomers upon incubation with high concentrations of n-dodecylphosphocholine (48). However, these proteins differ in that they are not inactivated in a ligand-bound oligomeric form. Therefore, PlaB represents the previously unobserved case of an enzyme that is inhibited by an allosteric mechanism that involves ligand-mediated oligomerization.

## Materials and Methods

**Bacterial Strains and DNA Techniques.** Bacterial strains, plasmids, and primers are listed in SI Appendix, Tables S4 and S5. *L. pneumophila* strain Corby was used for *plaB* cloning (49). Versions of PlaB were generated by means of the QuikChange Site-Directed Mutagenesis Kit (Stratagene) (SI Appendix, Table S4). Primers were obtained from Eurofins MWG Operon and IDT (SI Appendix,

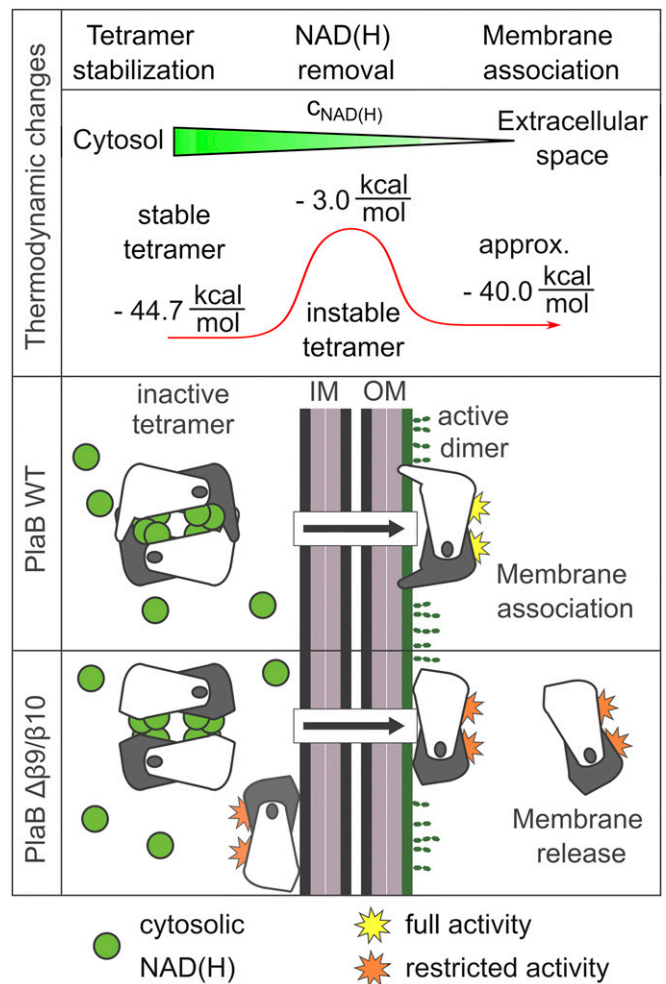


**Fig. 5.** Model of NAD(H)-dependent regulation of PlaB activity and membrane association. High concentrations of intracellular NAD(H) mediate tetramer formation of PlaB and thus inhibit lipolytic activity and presumably protect from bacterial lysis. It is assumed that, upon PlaB export, NAD(H) concentrations drop and PlaB tetramers dissociate into dimers. Dimers will subsequently associate with the bacterial OM and be presented in the active form. The tetramer is stabilized by NAD(H) ( $\Delta G = -44.7$  kcal/mol) but renders unstable without the ligand ( $-3.0$  kcal/mol). In the dimeric form of PlaB, β-9/β-10 becomes accessible for membrane interaction. The expected energy gain upon membrane association of two PlaB dimers with two β-9/β-10 elements each can be estimated to amount to approximately  $-40$  kcal/mol, and therefore membrane association is thermodynamically supported. Although NAD(H) still stabilizes the PlaB Δβ-9/β-10 tetramer, the deletion mutant is impaired in terms of tetramer stability, OM localization, and activity.

**Table S5.** The bacterial strains were cultivated in lysogeny broth media containing 100 μg/mL ampicillin or 30 μg/mL chloramphenicol (for *E. coli*) or buffered yeast extract (BYE) broth when required containing 6 μg/mL chloramphenicol (for *L. pneumophila*).

**Protein Expression and Purification.** PlaB for crystallization was produced as N terminally Strep-tagged inactive Strep-PlaB D203N as described previously (16). Briefly, protein was expressed in *E. coli* BL21 (pKK21), using 50 μM isopropyl 1-thio-D-galactopyranoside (IPTG) for induction. Seleno-L-methionine labeling was achieved by growing the bacteria in M9 minimal medium supplemented with 50 mg/L seleno-L-methionine (SeMet) and inducing with 50 μM IPTG overnight at 20 °C. Purification involved Strep-Tactin affinity and size-exclusion chromatography, followed by concentration to 10 mg/mL and storage at  $-80$  °C until further usage. For activity and localization analyses, PlaB and variants were expressed using 0.1 mM IPTG for induction and purification by means of Strep-Tactin affinity and size-exclusion chromatography.

**SEC-MALS.** SEC-MALS experiments were performed on a chromatography system equipped with a Superdex 200 Increase 10/300 GL SEC column, a miniDAWN TREOS MALS detector, and an Optilab T-REX refractometer (Wyatt Technology Corp.) The column was equilibrated with 150 mM NaCl, 50 mM Tris (pH = 8), and different volumes of protein solution at 10 mg/mL were analyzed. Data were processed with the Astra software package (Wyatt Technology Corp.)

**TSA.** TSAs were performed by mixing 5  $\mu$ L protein solution at 2 mg/mL with 5  $\mu$ L SYPROorange (1:50 diluted from 5,000 $\times$  stock solution, Invitrogen), 5  $\mu$ L eightfold buffer (1,200 mM NaCl and 400 mM Tris pH = 8), and 35  $\mu$ L RUBIC Additive Screen (Molecular Dimensions) in a 96-well plate. Data were collected with a C1000 Touch Thermal Cycler, equipped with a CFX96 Real-Time System from 4 to 95  $^{\circ}$ C in 1  $^{\circ}$ C increments. TSA data were analyzed with the software BIO-RAD CFX96 Manager 3.1 (BIO-RAD).

**Crystallization and Data Collection.** Initial crystallization conditions were identified with the vapor diffusion method in sitting drops consisting of 200 nL protein solution at a concentration of 1 to 6 mg/mL mixed with the same volume of precipitant and equilibrated against 60  $\mu$ L reservoir at 20  $^{\circ}$ C. Precipitants yielding crystals were optimized in grid and random screens. Microseeding experiments were performed with an OryxNano liquid dispenser (Douglas Instruments) using 100 nL seed stock of native PlaB crystals broken up in 500  $\mu$ L of the corresponding reservoir and 300 nL SeMet PlaB at 4 mg/mL mixed with 200 nL precipitant solution. Crystals were further optimized by preincubating the protein with 1 mM thio-nicotinamidinucleotide (SNAD). Diffraction data collection proceeded with crystals obtained with precipitants consisting of 100 mM Tris (pH = 8.5), 8.33% glycerol, 10.8% 2-propanol (native PlaB) and 77.8 mM NaSCN, 1.67% glycerol, 5.44% PEG400, 11.6% 2-propanol, and 4.11% tacsimate (SeMet PlaB). Crystals were cryoprotected in mother liquor supplemented with 10% (vol/vol) (2R,3R)-(-)-2,3-butandiol before flash cooling in liquid nitrogen. Diffraction data were collected on beamlines BL14.2 [synchrotron BESSYII, Helmholtz Zentrum Berlin (50)], P11 [synchrotron PETRAIII, Deutsches Elektronen-Synchrotron (DESY) (51)] and PXIII/X06DA [synchrotron Swiss Light Source (SLS), Paul Scherrer Institute (52)]. Indexing and integration was achieved with XDS, and scaling involved AIMLESS or STARANISO (53–57), as summarized in *SI Appendix, Table S1*.

**Structure Determination and Refinement.** Initial phases were derived from single anomalous dispersion differences in diffraction data of a crystal of SeMet-labeled PlaB collected at the K-absorption edge of selenium. Heavy atom positions were identified with hkl2map (55) and forwarded to phenix.phaser of the PHENIX software suite (58). An initial model was obtained with phenix.autobuild and completed manually in Coot (59) from the CCP4 software suite (56). Further refinement involved alternating rounds of manual adjustments and optimization in phenix.refine. Model statistics are provided in *SI Appendix, Table S1*. Coordinates and structure factor amplitudes have been deposited in the Protein Data Bank (60) under accession code 6zth [seleno-L-methionine-containing structure with low-occupancy NAD(H)] and 6zti (unlabeled PlaB-containing SNAD at full occupancy). Molecular structures are displayed with PyMOL (61).

**Determination of Lipolytic Activities.** Purified protein, bacterial lysates, or culture supernatants of *E. coli* BL21 expressing PlaB or its versions were incubated with different lipids (dipalmitoyl phosphatidic acid [PA], dipalmitoyl phosphatidylcholine [PC], dipalmitoyl phosphatidylglycerol [PG], dipalmitoyl phosphatidylethanolamine [PE], dipalmitoyl phosphatidylserine [PS], 1-monopalmitoyl-lysophosphatidic acid [LPA], 1-monopalmitoyl-lysophosphatidylcholine [LPC], 1-monopalmitoyl-lysophosphatidylglycerol [LPG], 1-monopalmitoyl-lysophosphatidylethanolamine [LPE] [Avanti Polar Lipids, Inc.], and dipalmitoyl phosphatidylinositol [PI] [MoBiTec]), 3 mM Na<sub>2</sub>S<sub>2</sub>O<sub>8</sub>, 0.5% Triton X-100, and 20 mM Tris HCl (pH = 7.2) as described previously. Prior to incubation, the lipids were vortexed for 15 min at 37  $^{\circ}$ C and then exposed to ultrasonication (Sonoplus, Bandelin, sonotrode MS73) three times, for 15 s each, at cycle 4  $\times$  10% with the power set to 65%. The release of fatty acids was determined using the NEFA-HR (2) assay (Wako Fujifilm) as described previously (15).

**Liposome Cosedimentation Assay.** Liposomes were generated by using PG or PC (Avanti Polar Lipids, Inc.). A total of 8 mM of the lipid was resuspended in 40 mM Tris HCl (pH = 7.5) with 10% glycerol and incubated for 1 h at 37  $^{\circ}$ C at 250 rpm. The lipid suspension was sonicated with following parameters: 3  $\times$  15 s at cycle 4 and 65% intensity (Bandelin Sonoplus, sonotrode MS73). A total of 1 mL of 1 mM liposome suspension was incubated with 0.3  $\mu$ M purified PlaB D203N, PlaB D203N  $\Delta$ p9/10 for 30 min followed by ultracentrifugation at 38,800 rpm at 4  $^{\circ}$ C for 30 min. The supernatants were 10-fold

concentrated (Amicon Ultra-4 10K Centrifugal Filter Devices, Merck), and the pellet was resuspended in 100  $\mu$ L 40 mM Tris HCl (pH = 7.5). Detection of Strep-PlaB was performed via Western blot analysis (StrepMAB-ClassiC, horseradish peroxidase [HRP] conjugate, Iba).

**PlaB External Association to *L. pneumophila*.** *L. pneumophila*  $\Delta$ plaB was grown over night in BYE to optical density (OD<sub>600</sub>)  $\sim$ 3. Bacterial cells were harvested and washed 2 $\times$  with 40 mM Tris HCl (pH = 7.5). A total of 1 mL of the cells was incubated with 0.3  $\mu$ M purified PlaB or PlaB  $\Delta$ p9/10 for 10 min at 37  $^{\circ}$ C. Cells were washed 10 $\times$  with 1 mL 40 mM Tris HCl. The cell pellet was lysed in 50  $\mu$ L 40 mM Tris HCl (pH = 7.5) with 10 mg/mL lysozyme and Triton X-100 (0.1%) and was incubated at 37  $^{\circ}$ C for 30 min. After lysis, the volume of the sample was adjusted to 1 mL with Tris HCl. The final lysates and supernatants of all wash steps were used for Western blot analysis detecting Strep-PlaB (StrepMAB-ClassiC, HRP conjugate, Iba).

**Bacterial Cell Fractionation.** Separation of inner and OMs of *E. coli* and *L. pneumophila* strains was performed with changes according to Roy and Isberg (62). For *E. coli*, 100 mL of cell culture were induced at an OD<sub>600</sub> = 0.8 with 0.1 mM IPTG and incubated for 3 h at 37  $^{\circ}$ C and 250 rpm. For *L. pneumophila*, the induced culture was grown until late exponential phase. The culture was adjusted to OD<sub>600</sub> = 1. The pellet of 100 mL was resuspended in 1 mL cold fractionation buffer (40 mM Hepes, 0.1 mM ethylenediaminetetraacetic acid, 1 $\times$  Complete Protease Inhibitor Mixture [Roche Sigma]) and the pellet of 1 mL lysed with Bug Buster (pellet sample) (Bug Buster Master Mix, Novagen Merck). For lysis, the cells were sonified for 3 min (30% amplitude, 0.4-s pulse, Bandelin Sonoplus HD2070). The supernatant (soluble components), obtained after centrifugation at 10,000  $\times$  g for 20 min at 4  $^{\circ}$ C, was ultracentrifuged at 100,000  $\times$  g for 1 h at 4  $^{\circ}$ C. The pellet (membrane fraction) was washed and resuspended in 1 mL cold fractionation buffer, and 2% Triton X-100 and 30 mM MgCl<sub>2</sub> were added (62, 63). After 5 min at room temperature, the pellets were resolved in an ultrasound bath (5 min, room temperature Bandelin Sonorex Super RK 103 H), and ultracentrifuged at 100,000  $\times$  g for 2 h at 4  $^{\circ}$ C. The supernatant (inner membrane fraction) was separated from the pellet (OM), which was dissolved in 1 mL fractionation buffer using an ultrasound bath for 5 min. Fractions were analyzed by means of Western blotting detecting Strep-PlaB (StrepMAB-ClassiC, HRP conjugate, Iba), the OM control proteins OmpA [ $\alpha$ -OmpA was kindly provided by Nemani V. Prasadarao, Children's Hospital Los Angeles, Los Angeles, CA (64)] or MOMP ( $\alpha$ -MOMP, MONOFLUO *L. pneumophila* IFA Test Kit, BioRad), the inner membrane control protein LepB [antibody kindly provided by Gunnar von Heinje, Stockholm University, Stockholm, Sweden (65)], and the cytosolic control proteins DnaK (DnaK monoclonal antibody, Enzo Life Sciences).

**Detection of PlaB Localization and Bacterial Lysis during Bacterial Growth Kinetics.** The *E. coli* BL21 and the *L. pneumophila* strains were grown to an OD<sub>600</sub> of 1.0 and expression was induced by the addition of 0.1 mM IPTG. At distinct optical densities, 1 mL samples were pelleted. The supernatants were concentrated 10 times with Amicon Ultra 0.5 mL Centrifugal Filters ( $\sim$ 10 K, Merck) and boiled with 1 $\times$  sodium dodecyl sulfate (SDS) loading buffer. The cell pellets were resuspended in 50  $\mu$ L 40 mM Tris HCl (pH = 7.5) with lysozyme (10 mg/mL) and Triton X-100 [0.1% vol/vol] and incubated at 37  $^{\circ}$ C for 30 min. After lysis, the volume of the samples was adjusted to 1 mL with 40 mM Tris HCl (pH = 7.5) and sample aliquots for SDS-polyacrylamide gel electrophoresis (PAGE) and Western blotting analysis were prepared. Strep-PlaB and cytoplasmic DnaK in *E. coli* strains was detected by StrepMAB-ClassiC (HRP conjugate, Iba) and DnaK (DnaK monoclonal antibody, Enzo Life Sciences) antibodies. For detection of 4 $\times$ HA-PlaB and cytoplasmic ICDH of *L. pneumophila*,  $\alpha$ -HA.11 Epitope Tag (BioLegend) and  $\alpha$ -ICDH [kindly provided by Ralph Isberg, Tufts University, Boston, MA (66)] antibodies were used.

**Data Availability.** Crystal structure data have been deposited in Protein Data Bank (accession nos. 6zth and 6zti).

**ACKNOWLEDGMENTS.** We acknowledge the staff at beamlines P11 (PETRAIII, DESY Hamburg, Germany), BL14.2 at synchrotron BESSYII (Helmholtz Zentrum Berlin, Germany), and PXIII/X06DA at SLS (Paul Scherrer Institute, Villigen, Switzerland) for providing us access to their facilities. We thank Dirk Heinz and Sally Pham for work in the early stages of structural analysis; Ute Curth for consultations regarding oligomer analysis; and Christian Galisch, Susanne Karste, and Ute Strutz for excellent technical assistance. This work was supported by funds from the Deutsche Forschungsgemeinschaft awarded to A.F. (FL359/4-2/3) and W.B. (281361126/GRK2223).

1. M. Flores-Díaz, L. Monturiol-Gross, C. Naylor, A. Alape-Girón, A. Flieger, Bacterial sphingomyelinases and phospholipases as virulence factors. *Microbiol. Mol. Biol. Rev.* **80**, 597–628 (2016).
2. H. Sato *et al.*, The mechanism of action of the *Pseudomonas aeruginosa*-encoded type III cytotoxin, ExoU. *EMBO J.* **22**, 2959–2969 (2003).
3. R. M. Phillips, D. A. Six, E. A. Dennis, P. Ghosh, In vivo phospholipase activity of the *Pseudomonas aeruginosa* cytotoxin ExoU and protection of mammalian cells with phospholipase A2 inhibitors. *J. Biol. Chem.* **278**, 41326–41332 (2003).
4. M. H. Diaz, A. R. Hauser, *Pseudomonas aeruginosa* cytotoxin ExoU is injected into phagocytic cells during acute pneumonia. *Infect. Immun.* **78**, 1447–1456 (2010).
5. A. H. Gaspar, M. P. Machner, VipD is a Rab5-activated phospholipase A1 that protects *Legionella pneumophila* from endosomal fusion. *Proc. Natl. Acad. Sci. U.S.A.* **111**, 4560–4565 (2014).
6. N. Shohdy, J. A. Efe, S. D. Emr, H. A. Shuman, Pathogen effector protein screening in yeast identifies *Legionella* factors that interfere with membrane trafficking. *Proc. Natl. Acad. Sci. U.S.A.* **102**, 4866–4871 (2005).
7. G. A. Smith *et al.*, The two distinct phospholipases C of *Listeria monocytogenes* have overlapping roles in escape from a vacuole and cell-to-cell spread. *Infect. Immun.* **63**, 4231–4237 (1995).
8. A. Camilli, H. Goldfine, D. A. Portnoy, *Listeria monocytogenes* mutants lacking phosphatidylinositol-specific phospholipase C are avirulent. *J. Exp. Med.* **173**, 751–754 (1991).
9. D. H. Schmiel, V. L. Miller, Bacterial phospholipases and pathogenesis. *Microbes Infect.* **1**, 1103–1112 (1999).
10. W. C. Winn Jr, R. L. Myerowitz, The pathology of the *Legionella pneumonias*. A review of 74 cases and the literature. *Hum. Pathol.* **12**, 401–422 (1981).
11. M. Hiller, C. Lang, W. Michel, A. Flieger, Secreted phospholipases of the lung pathogen *Legionella pneumophila*. *Int. J. Med. Microbiol.* **308**, 168–175 (2018).
12. S. Mondino *et al.*, Legionnaires' disease: State of the art knowledge of pathogenesis mechanisms of *Legionella*. *Annu. Rev. Pathol.* **15**, 439–466 (2020).
13. E. Schunder *et al.*, Phospholipase PlabA is a new virulence factor of *Legionella pneumophila*. *Int. J. Med. Microbiol.* **300**, 313–323 (2010).
14. A. Flieger, K. Rydzewski, S. Banerji, M. Broich, K. Heuner, Cloning and characterization of the gene encoding the major cell-associated phospholipase A of *Legionella pneumophila*, plabA, exhibiting hemolytic activity. *Infect. Immun.* **72**, 2648–2658 (2004).
15. J. Bender *et al.*, Phospholipase PlabB of *Legionella pneumophila* represents a novel lipase family: Protein residues essential for lipolytic activity, substrate specificity, and hemolysis. *J. Biol. Chem.* **284**, 27185–27194 (2009).
16. K. Kuhle *et al.*, Oligomerization inhibits *Legionella pneumophila* PlabB phospholipase A activity. *J. Biol. Chem.* **289**, 18657–18666 (2014).
17. W. R. Finnerty, R. A. Makula, J. C. Feeley, Cellular lipids of the Legionnaires' disease bacterium. *Ann. Intern. Med.* **90**, 631–634 (1979).
18. G. M. Conover *et al.*, Phosphatidylcholine synthesis is required for optimal function of *Legionella pneumophila* virulence determinants. *Cell. Microbiol.* **10**, 514–528 (2008).
19. M. B. Fessler, R. S. Summer, Surfactant lipids at the host-environment interface metabolic sensors, suppressors, and effectors of inflammatory lung disease. *Am. J. Respir. Cell Mol. Biol.* **54**, 624–635 (2016).
20. E. Krissinel, K. Henrick, Inference of macromolecular assemblies from crystalline state. *J. Mol. Biol.* **372**, 774–797 (2007).
21. A. Rauwerdink, R. J. Kazlauskas, How the same core catalytic machinery catalyzes 17 different reactions: The serine-histidine-aspartate catalytic triad of  $\alpha/\beta$ -hydrolase fold enzymes. *ACS Catal.* **5**, 6153–6176 (2015).
22. J. Mindrebo, C. Nartey, Y. Seto, M. Burkart, J. Noel, Unveiling the functional diversity of the Alpha-Beta hydrolase fold in plants. *Curr. Opin. Struct. Biol.* **41**, 233–246 (2016).
23. F. I. Khan *et al.*, The lid domain in lipases: Structural and functional determinant of enzymatic properties. *Front. Bioeng. Biotechnol.* **5**, 16 (2017).
24. L. Holm, Benchmarking fold detection by DALI Lite v.5. *Bioinformatics* **35**, 5326–5327 (2019).
25. A. L. Swart, H. Hilbi, Phosphoinositides and the fate of *Legionella* in phagocytes. *Front. Immunol.* **11**, 25 (2020).
26. M. Holmquist, I. G. Clausen, S. Patkar, A. Svendsen, K. Hult, Probing a functional role of Glu87 and Trp89 in the lid of *Hemicola lanuginosa* lipase through transesterification reactions in organic solvent. *J. Protein Chem.* **14**, 217–224 (1995).
27. H. M. Khan *et al.*, A role for weak electrostatic interactions in peripheral membrane protein binding. *Biophys. J.* **110**, 1367–1378 (2016).
28. C. Grauffel *et al.*, Cation- $\pi$  interactions as lipid-specific anchors for phosphatidylinositol-specific phospholipase C. *J. Am. Chem. Soc.* **135**, 5740–5750 (2013).
29. M. S. Hindahl, B. H. Iglewski, Isolation and characterization of the *Legionella pneumophila* outer membrane. *J. Bacteriol.* **159**, 107–113 (1984).
30. W. J. Black, F. D. Quinn, L. S. Tompkins, *Legionella pneumophila* zinc metalloprotease is structurally and functionally homologous to *Pseudomonas aeruginosa* elastase. *J. Bacteriol.* **172**, 2608–2613 (1990).
31. S. F. Altschul, W. Gish, W. Miller, E. W. Myers, D. J. Lipman, Basic local alignment search tool. *J. Mol. Biol.* **215**, 403–410 (1990).
32. B. E. Suzek, Y. Wang, H. Huang, P. B. McGarvey, C. H. Wu; UniProt Consortium, UniRef clusters: A comprehensive and scalable alternative for improving sequence similarity searches. *Bioinformatics* **31**, 926–932 (2015).
33. R. Zallot, N. Oberg, J. A. Gerlt, The EFI web resource for genomic enzymology tools: Leveraging protein, genome, and metagenome databases to discover novel enzymes and metabolic pathways. *Biochemistry* **58**, 4169–4182 (2019).
34. C. Schleberger, P. Sachelaru, R. Brandsch, G. E. Schulz, Structure and action of a C-C bond cleaving  $\alpha/\beta$ -hydrolase involved in nicotine degradation. *J. Mol. Biol.* **367**, 409–418 (2007).
35. N. Pollak, C. Dölle, M. Ziegler, The power to reduce: Pyridine nucleotides–Small molecules with a multitude of functions. *Biochem. J.* **402**, 205–218 (2007).
36. Y. Zhou *et al.*, Determining the extremes of the cellular NAD(H) level by using an *Escherichia coli* NAD(+)-auxotrophic mutant. *Appl. Environ. Microbiol.* **77**, 6133–6140 (2011).
37. Q. Zhang, D. W. Piston, R. H. Goodman, Regulation of corepressor function by nuclear NADH. *Science* **295**, 1895–1897 (2002).
38. T. Yue *et al.*, How transmembrane peptides insert and orientate in biomembranes: A combined experimental and simulation study. *Phys. Chem. Chem. Phys.* **18**, 17483–17494 (2016).
39. K. L. May, T. J. Silhavy, The *Escherichia coli* phospholipase PldA regulates outer membrane homeostasis via lipid signaling. *mBio* **9**, 1–14 (2018).
40. R. E. Bishop, Structural biology of membrane-intrinsic  $\beta$ -barrel enzymes: Sentinels of the bacterial outer membrane. *Biochim. Biophys. Acta* **1778**, 1881–1896 (2008).
41. N. Dekker, Outer-membrane phospholipase A: Known structure, unknown biological function. *Mol. Microbiol.* **35**, 711–717 (2000).
42. C. Cantó, K. J. Menzies, J. Auwerx, NAD+ metabolism and the control of energy homeostasis—A balancing act between mitochondria and the nucleus. *Cell Metab.* **22**, 31–53 (2015).
43. H. J. Snijder *et al.*, Structural evidence for dimerization-regulated activation of an integral membrane phospholipase. *Nature* **401**, 717–721 (1999).
44. N. Griffon *et al.*, Identification of the active form of endothelial lipase, a homodimer in a head-to-tail conformation. *J. Biol. Chem.* **284**, 23322–23330 (2009).
45. P. T. Beernink, D. R. Tolan, Disruption of the aldolase A tetramer into catalytically active monomers. *Proc. Natl. Acad. Sci. U.S.A.* **93**, 5374–5379 (1996).
46. T. W. Traut, Dissociation of enzyme oligomers: A mechanism for allosteric regulation. *Crit. Rev. Biochem. Mol. Biol.* **29**, 125–163 (1994).
47. P. A. Ropp, T. W. Traut, Purine nucleoside phosphorylase. Allosteric regulation of a dissociating enzyme. *J. Biol. Chem.* **266**, 7682–7687 (1991).
48. S. A. Sanchez, Y. Chen, J. D. Müller, E. Gratton, T. L. Hazlett, Solution and interface aggregation states of *Crotalus atrox* venom phospholipase A2 by two-photon excitation fluorescence correlation spectroscopy. *Biochemistry* **40**, 6903–6911 (2001).
49. R. I. Jepras, R. B. Fitzgeorge, A. Baskerville, A comparison of virulence of two strains of *Legionella pneumophila* based on experimental aerosol infection of Guinea-pigs. *J. Hyg. (Lond.)* **95**, 29–38 (1985).
50. U. Mueller *et al.*, The macromolecular crystallography beamlines at BESSY II of the Helmholtz-Zentrum Berlin: Current status and perspectives. *Eur. Phys. J. Plus* **130**, 141 (2015).
51. A. Burkhardt *et al.*, Status of the crystallography beamlines at PETRA III. *Eur. Phys. J. Plus* **131**, 56 (2016).
52. R. Bingel-Erlenmeyer *et al.*, SLS crystallization platform at beamline X06DA-A fully automated pipeline enabling in situ X-ray diffraction screening. *Cryst. Growth Des.* **11**, 916–923 (2011).
53. W. Kabsch, XDS. *Acta Crystallogr. D Biol. Crystallogr.* **66**, 125–132 (2010).
54. W. Kabsch, Integration, scaling, space-group assignment and post-refinement. *Acta Crystallogr. D Biol. Crystallogr.* **66**, 133–144 (2010).
55. T. Pape, T. R. Schneider, HKL2MAP: A graphical user interface for macromolecular phasing with SHELX programs. *J. Appl. Cryst.* **37**, 843–844 (2004).
56. M. D. Winn *et al.*, Overview of the CCP4 suite and current developments. *Acta Crystallogr. D Biol. Crystallogr.* **67**, 235–242 (2011).
57. I. J. Tickle *et al.*, STARANISO (United Kingdom Glob. Phasing Ltd., Cambridge, 2018).
58. P. D. Adams *et al.*, PHENIX: A comprehensive python-based system for macromolecular structure solution. *Acta Crystallogr. D Biol. Crystallogr.* **66**, 213–221 (2010).
59. P. Emsley, B. Lohkamp, W. G. Scott, K. Cowtan, Features and development of Coot. *Acta Crystallogr. D Biol. Crystallogr.* **66**, 486–501 (2010).
60. H. M. Berman *et al.*, The protein data bank. *Nucleic Acids Res.* **28**, 235–242 (2000).
61. Schrödinger, LLC, The PyMOL Molecular Graphics System (Version 2.4, Schrödinger, LLC, 2020).
62. C. R. Roy, R. R. Isberg, Topology of *Legionella pneumophila* DotA: An inner membrane protein required for replication in macrophages. *Infect. Immun.* **65**, 571–578 (1997).
63. C. Filip, G. Fletcher, J. L. Wulff, C. F. Earhart, Solubilization of the cytoplasmic membrane of *Escherichia coli* by the ionic detergent sodium-lauryl sarcosinate. *J. Bacteriol.* **115**, 717–722 (1973).
64. N. V. Prasadarao *et al.*, Outer membrane protein A of *Escherichia coli* contributes to invasion of brain microvascular endothelial cells. *Infect. Immun.* **64**, 146–153 (1996).
65. L. Vranckx, E. De Buck, J. Anné, E. Lammertyn, *Legionella pneumophila* exhibits plasminogen activator activity. *Microbiology (Reading)* **153**, 3757–3765 (2007).
66. M. Liu, G. M. Conover, R. R. Isberg, *Legionella pneumophila* EhC is required for efficient replication in tumour necrosis factor alpha-stimulated macrophages. *Cell. Microbiol.* **10**, 1906–1923 (2008).